Flexible polymers and thin rods far from equilibrium: Buckling dynamics

Leonardo Golubovic,* Dorel Moldovan,† and Anatoli Peredera
Department of Physics, West Virginia University, Morgantown, West Virginia 26506
(Received 21 June 1999; revised manuscript received 17 September 1999)

We investigate the dynamics of the classical Euler buckling instability of compressed objects such as flexible molecular chains and thin rods moving in a viscous medium. We find that flexible chains undergo a coarsening process self-similar in time. They develop a wavelike pattern whose amplitude and wavelength grow in time. We relate the buckling dynamics to phase ordering phenomena. The role of the order parameter here is played by the chain slope with respect to the straight initial chain configuration.

PACS number(s): 82.20.Mj, 05.70.Ln, 46.32.+x, 0.5.40.−a

I. INTRODUCTION

Solids under externally applied stresses and strains exhibit a variety of instabilities. A classical example is the well-known Euler buckling instability of a compressed rod which buckles out sideways, if the compressional strain ε exceeds the critical value $\varepsilon_c \sim L^{-2}$; L is the length of the rod [1,2]. Buckling of thin rods and plates is a common phenomenon in engineering practice and materials science. Thus, for example, elastic and plastic buckling deformations are major effects in currently interesting strain induced morphological transitions in heteroepitaxially grown semiconductor materials [3]. On the other hand, in complex fluid physics, a buckling instability of polymerized monolayers of insoluble amphiphiles adsorbed at the air-water interface was observed in recent experiments [4]. Buckling can be induced in a variety of ways, for example, simply by applying a compressional lateral strain to a membrane or a long chain of molecules. In practice, strains causing buckling are frequently of thermal origin [5]. Thus protective coating films or oxide scales on metals may buckle due to the difference in thermal expansion coefficients between the film and the substrate. Rods with hinged ends immersed in a fluid may buckle if the temperature of the fluid is raised. The temperature jump would expand a rod with free ends. It thus effectively induces a uniform compressive strain ε in a rod with fixed ends. If $\varepsilon > \varepsilon_c \sim L^{-2}$, such a thermally strained rod will buckle.

Historically, Euler's buckling instability is the very first example of bifurcation phenomena, and a paradigm for subsequent theories of phase transitions [1]. In itself, buckling involves a spontaneous symmetry breaking. Thus a compressed membrane may buckle either up or down (breaking of Z_2, Ising-type symmetry), whereas a compressed thin cylindrical rod or molecular chain may buckle out sideways in an arbitrary direction (breaking of the O_2 symmetry for rotations around the initial direction of the rod). So, buckling is a practically interesting analog of *phase ordering phenomena*. In this paper, we investigate the fundamentals of buckling dynamics, that is, we investigate *how* initially straight, strained molecular chains (or thin rods) evolve into a final buckled configuration. There is much interesting physics in the dynamics of buckling that has been anticipated recently [6,7]. Here we document this by molecular dynamics simulations of a flexible chain of molecules (''tethered chain''). We find that chain buckling dynamics has the nature of *phase ordering processes* such as the growth of ordered domains in magnetic systems [8,9] or unstable mound growth in molecular beam epitaxy [10–12]. The evolving chain's profile is like a wave characterized by a wavelength that grows, via a coarsening process, as a power of time. The amplitude (transverse width) of this wavelike chain pattern also grows as a power of time. The order parameter of this phase ordering process is the chain slope with respect to the straight initial chain configuration. Our results were briefly outlined in Ref. [6]. Our effort here is a part of broad recent interest in the dynamics of deformed objects, such as flexible polymers [13] and tethered membranes [14]. The present work on chain buckling under compression complements a previous study on straightening of polymers under tension [15], as well as studies of Goldstein and co-workers on elastohydrodynamics of filaments [16,17]. Finally, we note that the buckling dynamics of tethered membranes was also recently studied by two of us in Ref. [7].

The balance of our paper is as follows. In Sec. II, we discuss the model for the flexible molecular chains. In Sec. III, simulations of the overdamped buckling dynamics of molecular chains are presented. In Sec. IV, we propose a scaling theory of the buckling dynamics. Section V discusses chain buckling dynamics as a phase ordering process. In Sec. VI and the Appendix, we discuss inertial and noise effects on buckling dynamics. A summary and a discussion of related work are contained in Sec. VII.

II. MODEL OF FLEXIBLE MOLECULAR CHAINS

We focus our study on thin rods [1,2], and closely related long flexible chains of molecules [13]. In Fig. 1(a), we schematically depict a section of the flexible chain of molecules that we investigate in this paper. Here $\vec{R}_n$ is the position of the nth molecule along the chain. The potential energy for the interactions of the particles along the chain contains two terms: the usual nearest-neighbor bonding term (compressional energy) as well as the next-nearest-neighbor terms yielding the chain bending energy. That is,

*Present address: Department of Physics, Harvard University, Cambridge, MA 02138.
†Present address: Materials Science Division, Argonne National Laboratory, Argonne, IL 60439.

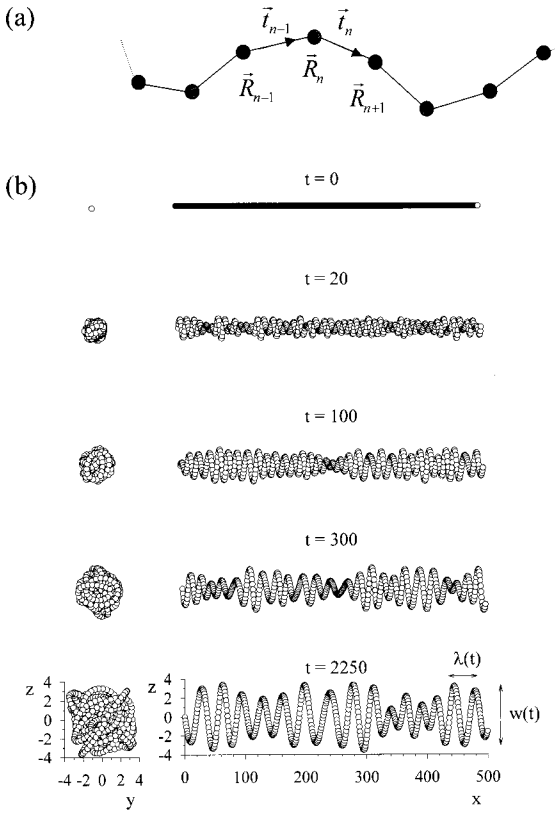

FIG. 1. (a) The model of the flexible molecular chain. (b) The time evolution of the molecular chain. We depict 550 out of 10 000 molecules comprising the chain. To depict undulations $\vec{R}_T(n,t)$ clearly, we used different scales for the transverse $\vec{R}_T=(R_y,R_z)$ and longitudinal $R_L=R_x$ molecular coordinates.

$$U=U_{\rm com}+U_{\rm bend}, \tag{2.1}$$

with the compressional energy

$$U_{\rm com}=\sum_n \Phi(|\vec{R}_{n+1}-\vec{R}_n|) \tag{2.2}$$

and the bending energy [given by a ferromagneticlike interaction between the nearest-neighbor bond vectors in Fig. 1(a)]

$$U_{\rm bend}=\frac{\kappa}{2}\sum_n (\vec{t}_{n+1}-\vec{t}_n)^2. \tag{2.3}$$

Here, $\vec{t}_n=(\vec{R}_{n+1}-\vec{R}_n)/|\vec{R}_{n+1}-\vec{R}_n|$ are the bond unit vectors, and κ is the chain bending rigidity modulus. The bonding potential $\Phi(|\vec{R}_{n+1}-\vec{R}_n|)$ in Eq. (2.2) is minimal when $|\vec{R}_{n+1}-\vec{R}_n|$ is equal to the bond length=1, in the units used here. We use

$$\Phi(|\vec{R}_{n+1}-\vec{R}_n|)=\frac{B}{2}e_n^2, \tag{2.4}$$

where B is the compresibility modulus, and e_n is the *internal strain* defined as

$$e_n=|\vec{R}_{n+1}-\vec{R}_n|-1. \tag{2.5}$$

Other forms of the bonding potential can be approximated by Eq. (2.4) in the vicinity of their minima at $e_n=0$. As discussed in the following, the scaling behavior of the buckling dynamics is, at long times, dominated by chain configurations for which $e_n\to 0$ as $t\to\infty$. Thus it is good enough to use the above simple model of the form of Φ. In the molecular dynamics simulations that we present here, $B=2.0$ and $\kappa=0.2$.

III. MOLECULAR DYNAMICS SIMULATIONS OF BUCKLING DYNAMICS OF FLEXIBLE CHAINS OF MOLECULES

The dynamical model studied here is the standard overdamped Rouse dynamics. This dynamical model basically corresponds to the motion of the molecular chain in a viscous medium, described by Langevin equations of motion:

$$\Gamma\frac{d\vec{R}_n}{dt}=-\frac{\partial U}{\partial\vec{R}_n}+\vec{\eta}_n(t). \tag{3.1}$$

Here $\vec{R}_n$ is the position of the nth molecule along the chain, Γ is a viscous friction coefficient, and $\vec{\eta}_n(t)$ is the thermal noise. To describe the chain dynamics, let us split the position vector of the nth molecule $\vec{R}_n$ into the transverse part $\vec{R}_T(n,t)$ (''undulations''), perpendicular to the initial straight chain direction, and the longitudinal part $R_L(n,t)$, along the initial chain direction. Chain ends are fixed (hinged), and at $t=0$ the chain was in a precompressed, straight configuration. That is, $R_L(n,t=0)=(1-\varepsilon)n$, and $\vec{R}_T(n,t=0)=0$. In our simulations, we used a 10% compressional external strain; that is, $\varepsilon=0.10$.

Here we focus on the dynamics without thermal noise (''*zero-temperature*'' dynamics), i.e., we set $\vec{\eta}_n(t)=0$ in Eq. (3.1), whereas $\Gamma=0.5$. Noise effects are discussed in Sec. VI. The only randomness used in this section was small initial random transverse displacements around the initially straight unstable equilibrium configuration (to enable chain start moving). Subsequently, buckling instability, due to negative internal strains, amplifies transverse displacements and produces a chaotic dynamics depicted in Fig. 1(b) from our simulations. Manifestly, the transverse displacements of the chain $\vec{R}_T(n,t)$ develop an *evolving* wavelike pattern characterized by a *time-dependent* structural length scale $\lambda(t)$ (''wavelength''). This $\lambda(t)$ grows with time via a coarsening process. Associated with this coarsening is a growth of the chain's transverse spread $w(t)$ (''width''); see Fig. 1(b).

We quantified the chain transverse spread $w(t)$ as the root-mean-square value of the transverse molecular displacements, that is, as

$$[w(t)]^2=\langle[\vec{R}_T(n,t)]^2\rangle. \tag{3.2}$$

Here and in the following, $\langle\cdots\rangle$ stands for the spatial average defined for any quantity $A(n,t)$ as $\langle A(n,t)\rangle=(1/N)\Sigma_{n=1}^{N}A(n,t)$, for a chain comprised of N molecules.

We extracted the chain wavelength $\lambda(t)$ from slope-slope correlation functions, that have a strong oscillatory character

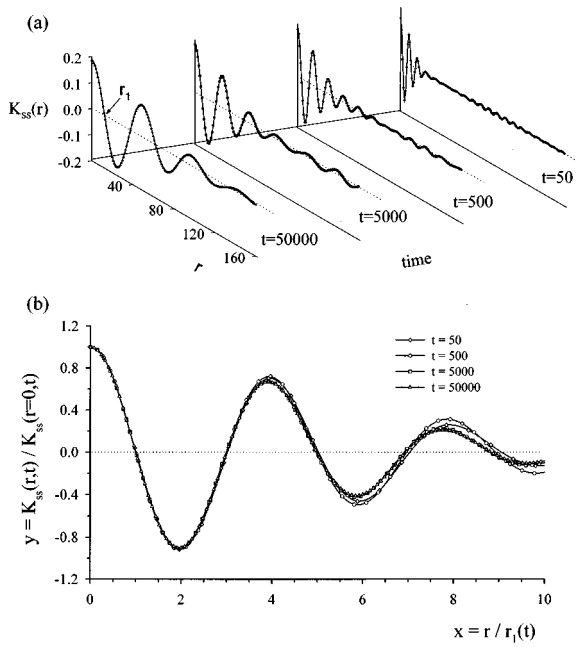

FIG. 2. (a) The slope-slope correlation functions $K_{ss}(r,t)$ vs r for various times t. Note that as $t\to\infty$, $K_{ss}(r=0,t)\to 2\varepsilon$ ($=0.2$ here, $\varepsilon=0.1$). (b) The self-similarity test for $K_{ss}(r,t)$ shows the collapse into a single curve $y=\psi(x)$ of the curves in (a). Here $y=K_{ss}(r,t)/K_{ss}(r=0,t)$ and $x=r/r_1(t)$, where $r_1(t)$ is the first zero of $K_{ss}(r,t)$.

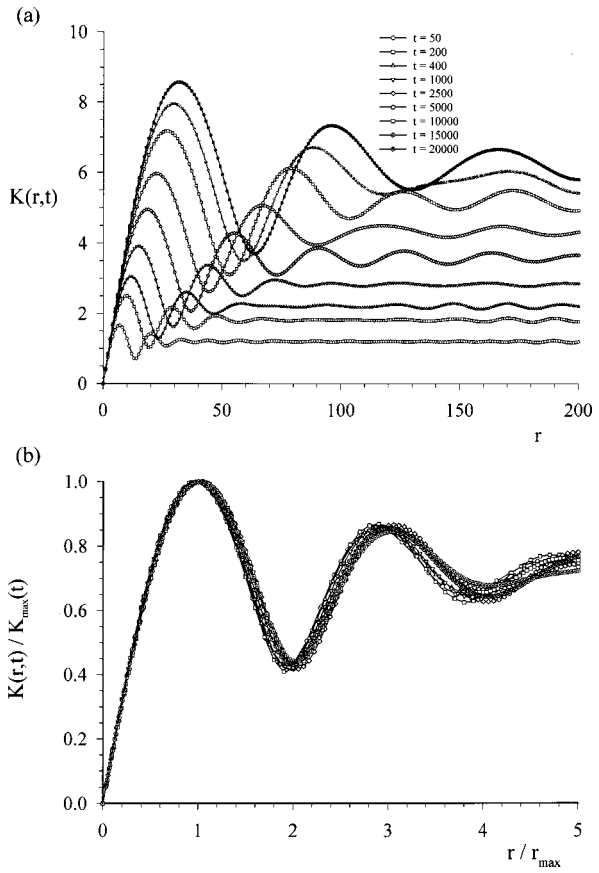

FIG. 3. (a) The time evolution of the displacement-displacement difference correlation functions $K(r,t)$ of the flexible molecular chain. (b) The rescaled displacement-displacement difference correlation functions. All of the correlation functions collapse into a single curve $y=f(x)$. Here $y=K(r,t)/K_{max}(t)$ and $x=r/r_{max}(t)$, where $K_{max}(t)$ is the maximum value of $K(r,t)$ which occurs at $r=r_{max}(t)$.

reflecting wavelike patterns in Fig. 1(b). We illustrate this in Fig. 2, that depicts the ''slope-slope'' correlation functions defined as

$$K_{ss}(r,t)=\langle \vec{V}_T(n+r,t)\cdot\vec{V}_T(n,t)\rangle, \tag{3.3}$$

where $\vec{V}_T(n,t)=\vec{R}_T(n+1,t)-\vec{R}_T(n,t)$ is the slope vector. These correlation functions, as well as the displacement-displacement difference correlation functions $K(r,t)$, defined as

$$K(r,t)=\langle[\vec{R}_T(n+r,t)-\vec{R}_T(n,t)]^2\rangle^{1/2}, \tag{3.4}$$

have an oscillatory character in the n dependence (see Fig. 3).

The chain wavelength $\lambda(t)$ can be extracted from the first zero $r_1(t)$ of $K_{ss}(r,t)$, via the relation $\lambda(t)=4r_1(t)$ [which can be rationalized by calculating $K_{ss}(r,t)$ for $\vec{R}_T(n,t)$ in the form of a simple harmonic wave with wavelength $\lambda(t)$]. We thus find that, at long times,

$$w(t)\sim t^{\beta}, \quad \lambda(t)\sim t^{n_c} \tag{3.5}$$

(see Fig. 4), with the exponents β and n_c both equal to 0.25 ± 0.01 from simulations of a three-dimensional chain of $N=10\,000$ molecules. Thus, within the accuracy, $\beta=n_c=\frac{1}{4}$.

We obtain additional insight into this scaling behavior by considering the chain's *total* potential energy U [Eq. (2.1)], which is the sum of the compressional energy U_{com} and bending energy U_{bend}. Figure 5(a) depicts the energies U, U_{com} and U_{bend} vs time. We see that, at long times,

$$U_{bend}(t)\sim\frac{1}{t^{\delta}}, \quad U_{com}(t)\sim\frac{1}{t^{\eta}} \tag{3.6}$$

with $\delta=0.50(4)$ and $\eta=1.02(2)$. As $\eta>\delta$, the net potential (elastic) energy U is, at long times, entirely in the bending energy, $U\approx U_{bend}\gg U_{com}$; see Fig. 5(a).

Figure 5(b) depicts the time evolution of the spatial average of the internal strain $e_n(t)$ [Eq. (2.5)]. It is important to notice that $\langle e_n\rangle<0$, indicating that the chain is in a compressed state at any time t. By Fig. 5(b) for long times, the internal strain relaxes as

$$\langle e_n\rangle\sim-\frac{1}{t^{\gamma}}, \tag{3.7}$$

with $\gamma=0.51(1)$. Note that, within the accuracy, one has the scaling relation $\eta=2\gamma$, where η is the exponent of the compressional energy decay; see Eq. (3.6). This can be easily rationalized as $U_{com}\sim\langle e_n^2\rangle$, if one further assumes that $\langle e_n^2\rangle\sim\langle e_n\rangle^2$.

The most apparent finding from these simulations is the presence of the growing length scales $w(t)$ and $\lambda(t)$. The typical length scale for chain transverse displacements $\vec{R}_T(n,t)$ is $w(t)$. Likewise, the typical length scale for n is

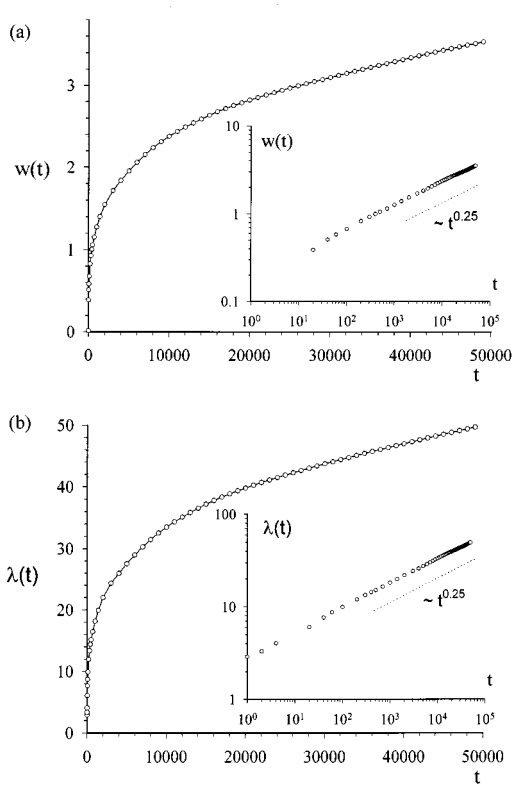

FIG. 4. (a) The time evolution of the transverse width $w(t)$ of the chain. The log-log plot gives the scaling $w(t)\sim t^{0.25}$. (b) The time evolution of the first zero crossing $r_1(t)$ of the slope-slope correlation function $K_{ss}(r,t)$. As discussed in the text, $r_1(t)$ is one quarter of the chain wavelength $\lambda(t)$. The log-log plot gives the scaling $\lambda(t)\sim t^{0.25}$. The linear plot indicates that $\lambda(t)$ starts from a nonzero value at $t=0$ as discussed in the text.

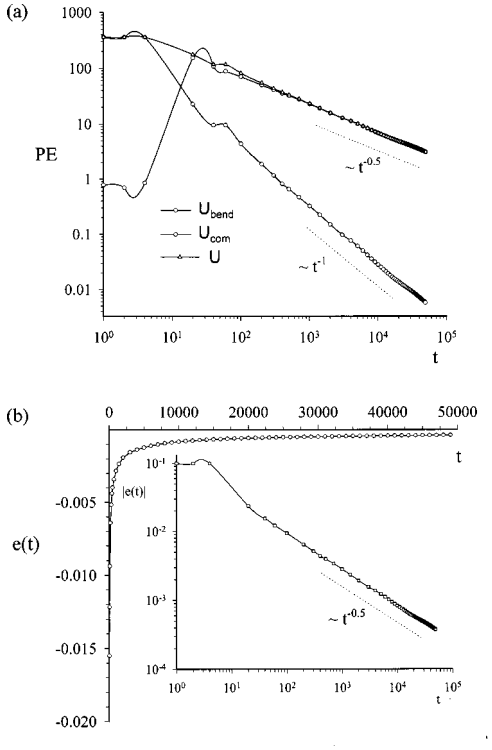

FIG. 5. (a) The time evolution of the chain total potential energy $U=U_{\rm bend}+U_{\rm com}$, bending energy $U_{\rm bend}$ and compressional energy $U_{\rm com}$. (b) The time evolution of the internal strain $e(t)$. Note that $e(t)<0$ for all times t.

the chain wavelength $\lambda(t)$, which reflects the periodiclike structure [see Fig. 1(b)] of $\vec{R}_T(n,t)$ versus n with the period $\lambda(t)$.

There is an apparent *self-similarity* we see in the chain dynamics. Indeed, from Fig. 1(b), we infer that chain configurations obtained at *different* long times look (statistically) the *same*, provided the transverse displacements $\vec{R}_T(n,t)$ are expressed in units of $w(t)$ [i.e., in terms of the ''dimensionless'' quantity $R_T(n,t)/w(t)$], and n is expressed in units of $\lambda(t)$ [i.e., in terms of the dimensionless quantity $n/\lambda(t)$]. Qualitatively speaking, one can say that the chain configurations depicted at various times in Fig. 1(b) are all of the form

$$\frac{R_T(n,t)}{w(t)}\approx\sin\left(2\pi\frac{n}{\lambda(t)}\right); \tag{3.8}$$

that is, $y=R_T(n,t)/w(t)$ is a wavelike function of $x=n/\lambda(t)$, with the period $\Delta x=1$. Statistical self-similarity can be checked by using the slope-slope correlation functions $K_{ss}(r,t)$ obtained at various times t [see Fig. 2(a)], and the displacement-displacement difference correlation functions $K(r,t)$ [see Fig. 3(a)]. In terms of the displacement-displacement difference correlation function $K(r,t)$ [Eq. (3.4)], which, in essence, measures the typical value of $|\vec{R}_T(n+r,t)-\vec{R}_T(n,t)|$, the statistical self-similarity means that the typical value of

$$\left|\frac{\vec{R}_T(n+r,t)}{w(t)}-\frac{\vec{R}_T(n,t)}{w(t)}\right| \tag{3.9}$$

can be expressed as a function of $r/\lambda(t)$. Therefore,

$$\frac{K(r,t)}{w(t)}=f\left(\frac{r}{\lambda(t)}\right) \tag{3.10}$$

for long times t. This self-similarity can be tested by plotting the rescaled quantity $y=K(r,t)/w(t)$, with $K(r,t)$ obtained at various times, versus the rescaled quantity $x=r/\lambda(t)$. If the self-similarity holds, all curves thus obtained should ''*collapse*'' into a single scaling function $y=f(x)$. We did in fact test this, by using the correlation functions $K(r,t)$ obtained at different times in Fig. 3(a). Already from Fig. 3(a), we see that these correlation functions, though obtained at different times, look similar in shape and may collapse into a single curve after a rescaling. For convenience, we did this rescaling by using $y=K(r,t)/K_{\max}(t)$ and $x=r/r_{\max}(t)$. Here $K_{\max}(t)$ is the maximum value of $K(r,t)$ which occurs at some value of $r=r_{\max}(t)$. If the self-similarity holds, all the curves thus constructed should collapse into a single curve $y=\Phi(x)$, where Φ is a scaling function [Φ is identical to f in Eq. (3.10) up to a simple rescaling]. It appears that this is the case, as documented in Fig. 3(b) [note that $\Phi(1)=1$, by the definition of the rescaling procedure]. Therefore, the statistical self-similarity of the flexible chain buckling dynamics is well confirmed by our simulation results.

An additional check of the self-similarity can be made by considering the slope-slope correlation functions [Eq. (3.3)] obtained at different times; see Fig. 2(a). The slope vector

$\vec{V}_T(n,t)=\partial\vec{R}_T/\partial n$ has the characteristic value $v(t)=w(t)/\lambda(t)$, inferred by looking at a typical chain configuration in Eq. (3.8). In the spirit of the statistical self-similarity, correlation of $\vec{V}_T(n,t)/v(t)$ with $\vec{V}_T(n+r,t)/v(t)$ should be a function of $r/\lambda(t)$ only; that is,

$$\frac{K_{ss}(r,t)}{v^2(t)}=f_{ss}\left(\frac{r}{\lambda(t)}\right), \tag{3.11}$$

where $f_{ss}(x)$ is a scaling function. In particular,

$$K_{ss}(r=0,t)=\langle(\vec{V}_T)^2\rangle=\left\langle\left(\frac{\partial\vec{R}_T}{\partial n}\right)^2\right\rangle=v^2(t)f_{ss}(0). \tag{3.12}$$

From the simulations, we see that $K_{ss}(r=0,t)$ saturates to a finite value at long times [see Fig. 2(a) at $r=0$]. This feature of the slope-slope correlation functions can be rationalized in terms of Eq. (3.12) as $v(t)=w(t)/\lambda(t)$, and $w(t)$ and $\lambda(t)$ are both $\sim t^{0.25}$ at *long* times. This is further discussed in Sec. IV, where we find $K_{ss}(r=0,t)=\langle(\partial\vec{R}_T/\partial n)^2\rangle\approx 2\varepsilon$ for $\varepsilon\ll 1$, at long times. Thus the self-similarity of $K_{ss}(r,t)$ is simply the statement that, at long times, all the curves in Fig. 2(a) are identical up to a time-dependent rescaling along the r axes *only*. The dynamics of correlations $K_{ss}(r,t)$ of the slope vector $\vec{V}_T=\partial\vec{R}_T/\partial n$ is thus identical to the dynamics of order parameter correlations in the phase ordering processes [8,9] with the chain *slope* $\vec{V}_T$ playing the role of the *order parameter* here. Indeed, the scaling form of $K_{ss}(r,t)$ in Eq. (3.11) is equivalent to the basic scaling form of the order parameter correlations in the phase ordering processes [8,9]. Figure 2(b) gives the basic test of the self-similarity of $K_{ss}(r,t)$, as suggested in Eq. (3.11). There we plot $y=K_{ss}(r,t)/K_{ss}(r=0,t)$ vs $x=r/r_1(t)=4r/\lambda(t)$ [as before, $r_1(t)=\lambda(t)/4$ is the first zero of $K_{ss}(r,t)$]. We see that the slope-slope correlation functions obtained at various times indeed collapse into a single scaling function $y=\psi(x)$ [$\psi(0)=1$ and $\psi(1)=0$, by the construction of the rescaling procedure]. Moreover, as to standard phase ordering phenomena, our scaling function $\psi(x)$ has a pronounced oscillatory character reflecting the presence of the structural length scale $\lambda(t)$.

Our simulations thus elucidate the nature of the classical Euler instability dynamics of a precompressed rod. It is a coarsening process characterized by a growing structural length scale $\lambda\sim t^{n_c}$. At long times $t\sim L^{1/n_c}$, this length scale becomes comparable to the rod length L, and then one recovers the usual picture of a buckled flexible chain. We find that the dynamics of the buckling instability has the nature of a phase ordering process [8–11]. It is a stochastic coarsening process statistically self-similar in time. As in phase ordering phenomena, stochastic dynamics here is produced by chain nonlinearities and the presence of many degrees of freedom rather than by thermal noise, which we switched off in the simulations presented in this section. Associated with this coarsening process is the growing transverse width of the rod $w(t)\sim t^{\beta}$, with $\beta=n_c$. Such a growth of $w(t)$ with $\beta=n_c$ makes buckling dynamics strikingly similar to the interfacial coarsening processes recently found to occur in molecular beam epitaxy (MBE) (so called pyramidal or mound growth [10–12]). In the MBE growth as well as in the present elastic problem, the evolving manifold (surface or line) develops a nonzero slope with respect to the initial straight configuration. The chain slope plays the role of the order parameter in this phase ordering process.

The similarity of the present problem to the MBE pyramidal growth is also reflected in the form of the displacement-displacement difference correlation function $K(r,t)$. This function behaves similarly to the height-height difference correlation function during the pyramidal growth. Indeed, for $r\ll\lambda(t)$, we see from Fig. 3 that $K(r,t)$ is nearly a *linear* function of r. That is,

$$K(r,t)\sim r^{\alpha}, \tag{3.13}$$

with $\alpha=1$. On the other hand, for $r\gg\lambda(t)$ the correlation function $K(r,t)$ saturates, in an oscillatory fashion, to the value $K(r=\infty,t)=\sqrt{2}w(t)$. Features such as $\alpha=1$, and an oscillatory behavior of $K(r,t)$, also occur in the MBE pyramidal growth [10–12].

Let us discuss the numerical prefactor in Eq. (3.13). By writing $\vec{R}_T(n+r,t)-\vec{R}_t(n,t)\approx r[\partial\vec{R}_T(n,t)/\partial n]=r\vec{V}_T(n,t)$ [$r\ll\lambda(t)$], and from Eqs. (3.3) and (3.4) we have

$$K(r,t)\approx[K_{ss}(r=0,t)]^{1/2}r=\left\langle\left(\frac{\partial\vec{R}_T}{\partial n}\right)^2\right\rangle^{1/2}r \tag{3.14}$$

for $r\ll\lambda(t)$. As noted above [see Eq. (3.12)], the prefactor of r in the Eq. (3.14) saturates at long times to a constant. In fact, in Sec. IV, we show that $K_{ss}(r=0,t=\infty)=K(\varepsilon)$, with $K(\varepsilon)\cong 2\varepsilon$, for $\varepsilon\ll 1$. Thus, for $r\ll\lambda(t)$,

$$K(r,t)\approx\sqrt{K(\varepsilon)}r. \tag{3.15}$$

On the other hand, by using the scaling forms (3.10) and (3.11), for $r\ll\lambda(t)$,

$$K(r,t)\approx C\frac{w}{\lambda}r; \tag{3.16}$$

here $C=f'(0)=\sqrt{f_{ss}(0)}$ is a numerical constant. From Eqs. (3.15) and (3.16), $w/\lambda=[\sqrt{K(\varepsilon)}/C]$. As $K(\varepsilon)\cong 2\varepsilon$ for $\varepsilon\ll 1$ (see Sec. IV), one has $V_T=\partial R_\perp/\partial n\approx w/\lambda\sim\sqrt{\varepsilon}$, for a small ε.

In Sec. IV, we will address the dynamics of the buckling instability by a scaling-type analysis. This yields, for example, the coarsening exponents $n_c=\beta=0.25$ for the chain buckling dynamics in the presence of the viscous friction, in agreement with the results of the numerical simulations of this section.

IV. SCALING THEORY OF THE BUCKLING DYNAMICS OF FLEXIBLE CHAINS OF MOLECULES

To explain our numerical results qualitatively, let us address the chain motion by a scaling-type analysis. To proceed, we split the position vector of the nth molecule $\vec{R}(n,t)$ into one longitudinal component $R_L(n,t)$ and two transverse components $\vec{R}_T(n,t)$ (''undulations''), along and perpendicular to the initial straight chain configuration, respectively. Next we introduce phononlike degrees of freedom.

This can be done, for example, by expanding around the *relaxed* straight chain configuration, by writing $R_L(n,t)=n+u(n,t)$. Alternatively, by expanding around the initial, *precompressed* straight configuration, we obtain another expression $R_L(n,t)=(1-\varepsilon)n+u'(n,t)$, where ε is the external compressional strain (for example, $\varepsilon=0.10$ in the simulations results of Sec. III). As the chain has fixed ends, we have the boundary conditions $R_L(N,t)=(1-\varepsilon)N$ and $R_L(0,t)=0$, or, in terms of the u' phonons, $u'(n,t)=0$ for $n=N$ and $n=0$. This can, alternatively, be expressed as

$$\left\langle \frac{\partial u'}{\partial n} \right\rangle = 0, \tag{4.1}$$

where, as in Sec. III, the average $\langle \cdots \rangle$ indicates the spatial average, defined for the quantity $A(n,t)$ as $\langle A(n,t)\rangle = (1/N)\int_0^N A(n,t)dn$. In contrast to $u'(n,t)$ phonons, the $u(n,t)$ phonons satisfy a more complicated boundary condition at $n=N$, of the form $u(N,t)=-\varepsilon N$, as $u(n,t)=-n\varepsilon+u'(n,t)$. Thus $\langle \partial u/\partial n\rangle = -\varepsilon$. In terms of the phonons and undulations, the internal strain (2.5) has the form

$$e(n,t) \approx \frac{\partial u}{\partial n} + \frac{1}{2}\left(\frac{\partial \vec{R}_T}{\partial n}\right)^2 \tag{4.2}$$

for small external strains $\varepsilon \ll 1$ considered here. Alternatively, as $\partial_n u = -\varepsilon + \partial_n u'$,

$$e(n,t) \approx -\varepsilon + \frac{\partial u'}{\partial n} + \frac{1}{2}\left(\frac{\partial \vec{R}_T}{\partial n}\right)^2. \tag{4.3}$$

In terms of phonons and undulations, the chain elastic potential energy reduces to

$$U = U_{\rm com} + U_{\rm bend}, \tag{4.4}$$

with

$$U_{\rm com} = \int_0^N dn \frac{B}{2}(e(n,t))^2 \tag{4.5}$$

and

$$U_{\rm bend} = \int_0^N dn \frac{\kappa}{2}\left(\frac{\partial^2 \vec{R}_T}{\partial n^2}\right)^2. \tag{4.6}$$

Next, let us focus on undulations $\vec{R}_T(n,t)$, which, by Eqs. (3.1), (4.4), (4.5), and (4.6), satisfy

$$\Gamma \frac{\partial}{\partial t}\vec{R}_T(n,t) = -\frac{\delta U}{\delta \vec{R}_T(n,t)} = \frac{\partial}{\partial n} B e(n,t) \frac{\partial}{\partial n}\vec{R}_T(n,t) - \kappa\left(\frac{\partial}{\partial n}\right)^4 \vec{R}_T(n,t); \tag{4.7}$$

here, as in Sec. III, we switched off the thermal noise. At the *early* stage of the chain evolution, Eq. (4.7) can be linearized, by approximating Eq. (4.3) with $e(n,t)\approx -\varepsilon$. Therefore,

$$\Gamma \frac{\partial}{\partial t}\vec{R}_T(n,t) \approx -B\varepsilon \frac{\partial^2}{\partial n^2}\vec{R}_T(n,t) - \kappa\left(\frac{\partial}{\partial n}\right)^4 \vec{R}_T(n,t). \tag{4.8}$$

For Eq. (4.8), we find harmonic wave modes of the form $R_T(n,t) \sim \mathrm{Re}\exp(\omega(k)t + ikn)$, with $\Gamma\omega(k) = B\varepsilon k^2 - \kappa k^4$. Thus all the modes with $k < \sqrt{B\varepsilon/\kappa}$ are unstable and will grow exponentially in time. The dominant, most unstable mode [maximizing $\omega(k)$] has $k = k_0 = \sqrt{B\varepsilon/2\kappa}$. The amplitude of this mode grows exponentially in time as $\exp(t/t_0)$, with

$$t_0 = \frac{1}{\omega(k_0)} = \Gamma \frac{B^2\varepsilon^2}{4\kappa}. \tag{4.9}$$

The wavelength of the fastest mode,

$$\lambda_0 = \frac{2\pi}{k_0} = 2\pi\sqrt{\frac{2\kappa}{B\varepsilon}}, \tag{4.10}$$

corresponds to the chain wavelength observed in our simulations at the early stage of the evolution [see Fig. 4(b) at $t \approx 0$; the initial wavelength is different from zero]. During the early stage, $t \ll t_0$, the internal strain is negative [$e(n,t) \approx -\varepsilon$, as noted above]. It will remain negative even during the subsequent, late stage for $t \gg t_0$, as discussed in the following [see Eq. (4.19)], and already documented by the simulations in Sec. III; see Fig. 5(b). Thus the buckling dynamics is, generally, driven by negative (compressional) internal strains. As the times goes on, the linearized theory (4.8) breaks down, and the nonlinear equation of motion (4.7) [with $e(n,t)$ as in Eq. (4.3)] must be considered to explain the most interesting results obtained from the simulations of Sec. III, such as the *power-low growth* of $\lambda(t)$ and $w(t)$ at long time scales. The early time behavior, with $\lambda(t)\approx\lambda_0$ and $w(t)\sim\exp(t/t_0)$, is, at long times $t \gg t_0$, replaced by a power-law growth of the form $\lambda(t)\sim t^{n_c}$ and $w(t)\sim t^{\beta}$.

To explain our numerical simulation results for the exponents n_c and β of these power laws, we address the nonlinear equations of the chain motion by a scaling-type analysis. It is based on the observation that the only characteristic *long length scales* at *long time* t are $\lambda(t)$ and $w(t)$, as suggested by the simulations of Sec. III, in particular by the collapse of the correlation functions [see Fig. 2(b) and 3(b)]. These simulations suggest that the typical scale for R_T is w, therefore, $R_T \sim w$. Likewise, the typical scale for n is λ, so $n \sim \lambda$ and $\partial/\partial n \sim 1/\lambda$. Thus, for example, $\partial R_T/\partial n \sim w(t)/\lambda(t)$, for a typical configuration of the chain, as clearly suggested by our simulations [see Fig. 1(b)]. Likewise, we have

$$\Gamma \frac{\partial R_T}{\partial t} \sim \Gamma \frac{w}{t} \tag{4.11}$$

for the typical value of the left hand side (LHS) of the nonlinear equation of motion (4.7), whereas the bending term on the right hand side (RHS) of Eq. (4.7), $\kappa(\partial/\partial n)^4 R_T$, behaves as

$$(\text{bending term}) \sim \kappa \frac{w}{\lambda^4}. \tag{4.12}$$

Likewise, the first, compressional term on the RHS of Eq. (4.7) behaves as $B(1/\lambda)e(1/\lambda)w$. Therefore,

$$(\text{compressional term}) \sim B \frac{ew}{\lambda^2}. \tag{4.13}$$

To proceed further, we assume that, in the late stage of the evolution, for $t \gg t_0$, the compressional and bending terms on the RHS of Eq. (4.7) are of the same order of magnitude. Thus both terms are of the order of the LHS of Eq. (4.7), that is, they are of the order $\Gamma w/t$; see Eq. (4.11). From Eqs. (4.12) and (4.13), we thus have

$$\Gamma \frac{w}{t} = \kappa \frac{w}{\lambda^4} = B \frac{|e| w}{\lambda^2}. \tag{4.14}$$

From Eq. (4.14), we see that

$$\lambda(t) = \left(\frac{\kappa t}{\Gamma} \right)^{1/4} \sim t^{1/4}. \tag{4.15}$$

Thus $\lambda(t) \sim t^{n_c}$, with

$$n_c = \frac{1}{4} = 0.25, \tag{4.16}$$

in perfect agreement with the numerical simulation result for n_c in Sec. III; see Fig. 4(b). From Eqs. (4.9) and (4.10), Eq. (4.15) can also be rewritten as

$$\lambda(t) = \left(\frac{t}{t_0} \right)^{1/4} \lambda_0. \tag{4.17}$$

Equation (4.14) also implies that the internal strain $e = -|e|$ behaves as

$$e = -\frac{\kappa}{B\lambda^2}. \tag{4.18}$$

By using Eqs. (4.9), (4.10), and (4.17), here

$$e = -\varepsilon \left(\frac{\lambda_0}{\lambda(t)} \right)^2 = -\varepsilon \left(\frac{t_0}{t} \right)^{1/2}. \tag{4.19}$$

Thus the internal strain decays as

$$e \sim -\frac{1}{\sqrt{t}}. \tag{4.20}$$

Therefore, the early regime, with $e \approx -\varepsilon$ for $t \ll t_0$ is, for $t \gg t_0$, replaced by a power-law decay [Eq. (4.20)], of the negative internal strain e that drives the dynamics of the buckling instability. By Eq. (4.20), we see that the compressional energy [Eq. (4.5)] $U_{\text{com}} \sim NBe^2/2 \sim e^2$ decays with time as

$$U_{\text{com}} \sim \frac{1}{t} \tag{4.21}$$

for $t \gg t_0$. These results for e and U_{com} are in perfect agreement with our numerical simulations [see Eqs. (3.7) and (3.6) and Fig. 5].

From Eqs. (4.1) and (4.3),

$$\langle e \rangle = -\varepsilon + \frac{1}{2} \left\langle \left(\frac{\partial \vec{R}_T}{\partial n} \right)^2 \right\rangle. \tag{4.22}$$

By using here $\partial R_T / \partial n \sim w(t)/\lambda(t)$, and Eq. (4.18), we find that

$$-\varepsilon + \frac{1}{2} \left(\frac{w(t)}{\lambda(t)} \right)^2 = -\frac{\kappa}{B(\lambda(t))^2}, \tag{4.23}$$

after dropping inessential numerical factors. From Eq. (4.23), we see that $w^2 = 2\varepsilon\lambda^2 - 2\kappa/B$, or, as $\kappa/B \sim \varepsilon\lambda_0^2$,

$$w^2(t) = 2\varepsilon[\lambda^2(t) - \lambda_0^2], \tag{4.24}$$

where λ_0 is the wavelength [Eq. (4.10)] found before for the *early* stage of evolution, $t \ll t_0$. At long times, $t \gg t_0$, one has $\lambda(t) \gg \lambda_0$ [see Eq. (4.17)]. Therefore, at these long time scales, from Eq. (4.24),

$$w(t) \approx \sqrt{2\varepsilon}\lambda(t). \tag{4.25}$$

As $\lambda(t) \sim t^{n_c}$, it follows, from Eq. (4.25), that $w(t) \sim t^{\beta}$, with the exponent

$$\beta = n_c = \frac{1}{4}, \tag{4.26}$$

in agreement with the result obtained by simulations in Sec. III.

The scaling behavior of the bending energy [Eq. (4.6)], numerically obtained in Sec. III [see Fig. 5(a)], can be now explained. Note that

$$\langle U_{\text{bend}} \rangle = \frac{N\kappa}{2} \left\langle \left(\frac{\partial^2 \vec{R}_T}{\partial n^2} \right)^2 \right\rangle = N\kappa \left(\frac{w}{\lambda^2} \right)^2 \sim t^{2\beta - 4n_c}. \tag{4.27}$$

Thus, from Eq. (4.26),

$$U_{\text{bend}}(t) \sim \frac{1}{\sqrt{t}}, \tag{4.28}$$

in agreement with our simulations [see Eq. (3.6), and Fig. 5(a)] at long times $t \gg t_0$. We recall that for early times $t \ll t_0$ the chain is nearly straight, and U_{bend} is small. As the time increases, the chain buckles and U_{bend} rapidly (exponentially with time) increases at early times [see Fig. 5(a)]. U_{bend} reaches its maximum at $t \approx t_0$. Finally, for $t > t_0$ the bending energy slowly decays as $1/\sqrt{t}$, as documented in the numerical simulations in Sec. III and derived analytically above from the scaling theory.

As $\langle e \rangle \to 0$ at long times, from Eq. (4.22),

$$\left\langle \left(\frac{\partial \vec{R}_T}{\partial n} \right)^2 \right\rangle = 2\varepsilon \tag{4.29}$$

for $t \gg t_0$. As $\vec{V}_T(n,t) = \partial \vec{R}_T / \partial n$, from Eqs. (4.29) and (3.3) we find that, at long times, the slope-slope correlation function (3.3) saturates at its origin to the value given by

$$K_{ss}(r=0,t) = \left\langle \left(\frac{\partial \vec{R}_T}{\partial n} \right)^2 \right\rangle = \langle (\vec{V}_T)^2 \rangle = K(\varepsilon), \quad (4.30)$$

with $K(\varepsilon) \cong 2\varepsilon$ for $\varepsilon \ll 1$. This saturation is also clearly documented by the numerical simulation results for $K_{ss}(r,t)$ in Sec. III [see Fig. 2(a)]. For $t \gg t_0$, slope-slope correlation function can thus be written as

$$K_{ss}(r,t) = K(\varepsilon) \psi \left(\frac{r}{\lambda(t)} \right), \quad (4.31)$$

where $\psi(x)$ is a scaling function [$\psi(0)=1$], as discussed in Sec. III.

V. BUCKLING DYNAMICS AS A PHASE ORDERING PROCESS

In this section, we present an analytic approach to the chain buckling dynamics. Buckling dynamics is a phase ordering process. It can thus be treated by employing phase ordering theories developed to explain phase ordering processes such as the growth of ordered domains in magnetic systems [8,9]. In our case, the order parameter is the chain slope vector $\vec{V}_T = \partial \vec{R}_T / \partial n$, whereas the size of the ordered domains is comparable to the chain wavelength $\lambda(t)$: at scales shorter than $\lambda(t)$, the chain is nearly straight with a constant slope, whereas at scales longer than $\lambda(t)$ the chain curves and the orientational order of $\vec{V}_T$ is lost [see Eq. (3.11) and Figs. 1 and 2]. In the following we use this fact to develop a phase ordering theory of the buckling dynamics. Our approach here is similar to a recent theory of Bray [9]. Basic ingredients of the phase ordering theory are the following.

(i) The fact that the chain slope $\vec{V}_T = \partial \vec{R}_T / \partial n$ is an order parameter here, with the correlations of the phase ordering form [9],

$$\langle \vec{V}_T(n_1,t) \cdot \vec{V}_T(n_2,t) \rangle = V^2(\infty) f_{ss} \left(\frac{n_1 - n_2}{\lambda(t)} \right), \quad (5.1)$$

as found from our simulations [see Eq. (3.11) and Fig. 2]; here $f_{ss}(0)=1$ and $V(\infty) = \sqrt{\langle [\vec{V}_T(t,n)]^2 \rangle_{t=\infty}} = (\xi(t)/\lambda(t))_{t=\infty}$ [$V(\infty) \cong \sqrt{2\varepsilon}$ for $\varepsilon \ll 1$; see Sec. IV].

(ii) The energy dissipation formula,

$$\frac{1}{\Gamma} \frac{dU}{dt} = -\sum_{n=1}^{N} \left(\frac{\partial \vec{R}_n}{\partial t} \right)^2, \quad (5.2)$$

implied by the equation of motion (3.1); here U is the chain potential energy [Eq. (2.1)]. In terms of the energy per particle $u = U/N$, Eq. (5.2) reads

$$\frac{1}{\Gamma} \frac{du}{dt} = -\left\langle \left(\frac{\partial \vec{R}_n}{\partial t} \right)^2 \right\rangle. \quad (5.3)$$

u is the sum of the bending and compressional contribution, $u = u_{bend} + u_{com}$, with $u_{bend} = (\kappa/2)(\partial^2 \vec{R}_T / \partial n^2)^2$ and $u_{com} = (B/2)e^2$ [see Eqs. (4.5) and (4.6)]. By using $u \approx u_{bend}$ in Eq. (5.3), [as $u_{bend} \gg u_{com}$ at long times; see Sec. III], and $\langle (\partial \vec{R}_n / \partial t)^2 \rangle \approx (dw/dt)^2$, we find

$$\frac{1}{\Gamma} \frac{d}{dt} u_{bend} \approx -\left(\frac{dw}{dt} \right)^2 \quad (5.4)$$

at long times. To proceed, we employ the phase ordering form of the order parameter correlations in Eq. (5.1), to find that

$$\left\langle \frac{\partial \vec{V}_T}{\partial n_1} \cdot \frac{\partial \vec{V}_T}{\partial n_2} \right\rangle = -\frac{V^2(\infty)}{\lambda^2(t)} f_{ss}'' \left(\frac{n_1 - n_2}{\lambda(t)} \right). \quad (5.5)$$

From Eq. (5.5) it follows that the average bending energy density is

$$u_{bend} = \frac{\kappa}{2} \left\langle \left(\frac{\partial^2 \vec{R}_T}{\partial n^2} \right)^2 \right\rangle = \frac{\kappa}{2} \left\langle \left(\frac{\partial \vec{V}_T}{\partial n} \right)^2 \right\rangle = C \frac{\kappa V^2(\infty)}{2\lambda^2(t)}. \quad (5.6)$$

Here $C = -f_{ss}''(0)$ is a numerical constant. By combining Eqs. (5.6) and (5.4), with $w(t) = V(\infty)\lambda(t)$, we find

$$\frac{1}{\Gamma} \frac{d}{dt} \left(\frac{\kappa}{2} \cdot \frac{V^2(\infty)}{\lambda^2} \right) = -\text{const}\, V^2(\infty) \left(\frac{d\lambda}{dt} \right)^2. \quad (5.7)$$

The differential equation (5.7) is easily integrated, yielding, at long times,

$$\frac{w(t)}{V(\infty)} = \lambda(t) = \text{const} \left(\frac{\kappa t}{\Gamma} \right)^{1/4}. \quad (5.8)$$

Thus $w(t) \sim \lambda(t) \sim t^{1/4}$, as well as [by Eq. (5.6)] $u_{bend} \sim 1/\lambda^2 \sim 1/\sqrt{t}$, in agreement with the corresponding results of Sec. IV.

Thus the phase ordering theory explains the observed values of the coarsening exponents, both for the buckling dynamics of molecular chains and rods (as discussed above) and for the buckling dynamics of tethered membranes (as discussed in our work [7]). We note that the buckling dynamics of tethered membranes and thin sheets is characterized by coarsening exponents that are different from those of molecular chains and thin rods. The major reason for this difference is the phenomenon of elastic energy localization, that occurs in the case of membranes [7], but does not occur in the case of flexible molecular chains. In buckling membranes, the elastic energy is localized on a smaller portion of the net membrane surface, occupied by a network of highly curved regions (ridges) [7]. In contrast to this, in buckling chains, there is no such energy localization, that is, the elastic energy is nearly uniformly distributed along the chains. In fact, Eq. (5.5) reflects the fact that the chain curvature is nearly uniformly distributed along the chain, i.e., that there are no highly curved, cusplike turns consuming large amounts of bending energy. Under this condition, $\lambda(t) \sim w(t)$ is the only length scale of interest here. The chain bending energy density can be then estimated simply as $\kappa(d^2R/dn^2)^2 \sim \kappa(w/\lambda^2)^2$, which is equivalent to Eq. (5.6)

[by recalling that $w(t)=V(\infty)\lambda(t)$]. Such a simple estimate breaks down for buckled tethered membranes due to the formation of ridge networks. There, essentially all elastic energy is localized within the ridges' width ($\sim\lambda^{2/3}$), which is an additional length scale of interest for coarsening process. In effect, tethered membranes have a different coarsening exponent $\lambda(t)\sim t^{n_c}$, with $n_c=3/11$ rather than $n_c=1/4$ [7]. We remark that, for membrane buckling dynamics, membrane slope correlations also have the phase ordering from [Eq. (5.1)]. However, for the tethered membrane case, the (asymptotic) scaling function f_{ss} in Eq. (5.1) has a cusp at the origin [i.e., the constant C in Eq. (5.6) is infinite]. This singularity reflects the presence of sharp domain walls, i.e., ridges across the surface of membrane (see Ref. [9] for similar situations in other phase ordering phenomena). In the case of molecular chains, collapsed slope-slope correlation functions do not have such a cusp at the origin, as documented by our simulations [see Fig. 2(b) at $x=0$]. Thus, for molecular chains, the constant C in Eq. (5.6) is finite. Physically, the absence of this cusp in correlations indicates the absence of highly curved, cusplike turns in the chain profile.

VI. INERTIAL AND NOISE EFFECTS

In light of our results, here we first discuss some other issues related to the dynamics of buckling instabilities. We address inertial and noise effects ignored in previous discussions, by considering the Langevin equation

$$m\frac{d^2\vec{R}_n}{dt^2}+\Gamma\frac{d\vec{R}_n}{dt}=-\frac{\partial U}{\partial\vec{R}_n}+\vec{\eta}_n(t), \tag{6.1}$$

which incorporates the effects of the molecular mass m. For transverse displacements R_T one would then obtain Eq. (4.7), with the LHS modified by the inclusion of the inertial term $m(d^2\vec{R}_T/dt^2)$. In the spirit of the scaling analysis of Sec. IV [see, eg., Eq. (4.11)], we find

$$\frac{m\dfrac{d^2R_T}{dt^2}}{\Gamma\dfrac{dR_T}{dt}}\sim\frac{m\dfrac{w(t)}{t^2}}{\Gamma\dfrac{w(t)}{t}}=\frac{m/\Gamma}{t}. \tag{6.2}$$

Thus, at long times $t\gg m/\Gamma$, the inertial term is irrelevant provided the viscous friction is present, $\Gamma\neq 0$. That is, the addition of the mass term would not qualitatively affect the coarsening exponents and other features of the long time behavior we found in Secs. III and IV. We checked this feature by numerically solving the equation of motion both with and without the inertial term included.

This irrelevance of the inertial effect holds provided the viscous friction is *present*. It is thus also interesting to see what would be the behavior with purely Newtonian chain dynamics [Eq. (6.1)] with no external friction and no noise (say, buckling dynamics in vacuum or a very dilute medium). This problem will be addressed elsewhere.

Let us go back to our Langevin dynamics [Eq. (3.1)] for a chain in a viscous medium *with* noise. In previous sections, we ignored the thermal noise term. One may thus ask the question whether the thermal noise is *irrelevant* for the coarsening (like inertial effects, as discussed above)? To address this question, let us compare, in the spirit of the scaling analysis of Sec. IV, the noise term and the viscous term in Eq. (3.1), by forming the ratio

$$Q=\frac{\eta^2}{\left(\Gamma\dfrac{d\vec{R}_T}{dt}\right)^2}. \tag{6.3}$$

In order for the noise to be insignificant, Q in Eq. (6.3) must be small. During the coarsening, $dR_T/dt\sim w/t$, whereas the scaling of the noise η can be found from its correlation $\langle\eta(n,t)\eta(0,0)\rangle=2\Gamma k_BT\delta(n)\delta(t)$. As $\delta(t)\sim 1/t$ and $\delta(n)\sim 1/n\sim 1/\lambda$, we find $\eta^2\sim\Gamma k_BT/\lambda t$. Thus, from Eq. (6.3), $Q=(\Gamma k_BT/\lambda t)/(\Gamma w/t)^2$. By expressing t and w here in terms of the chain wavelength $\lambda(t)$, by means of Eqs. (4.15), and (4.25), we find

$$Q(t)=\frac{\lambda(t)}{\lambda_{\max}}, \tag{6.4}$$

with

$$\lambda_{\max}=\varepsilon L_p=\varepsilon\frac{\kappa}{k_BT}. \tag{6.5}$$

Here L_p is the thermal *persistence length* of a free chain at the temperature T. Thus, as long as $\lambda(t)\ll\lambda_{\max}=\varepsilon L_p$, one has $Q(t)\ll 1$, and the noise can be ignored. The chain dynamics is then qualitatively the same as the one at $T=0$ that was described in previous sections. Obviously, the condition $Q(t)\ll 1$ will be violated at long enough time $t>t_{\max}$ with $t_{\max}$ defined via $Q(t_{\max})=1$, i.e., $\lambda_{\max}=\lambda(t_{\max})=(\kappa t_{\max}/\Gamma)^{1/4}=\lambda_0(t_{\max}/t_0)^{1/4}$ [see Eqs. (4.15) and (4.17)]. Thus, generally, if the chain is *long enough* with $N>\lambda_{\max}$, the noise will be relevant and start to dominate for $t>t_{\max}$. Note, however, that L_p diverges as $T\to 0$, and $\lambda_{\max}=\varepsilon L_p$ may thus easily exceed the rod size N. This is the case in any common mechanical engineering situation involving rodlike structures. There, the rod persistence length L_p is, in any practical situation, enormously larger than the rod size. Thus, for all practical purposes of the *common* mechanical engineering, thermal noise has insignificant effects on the buckling dynamics. There the buckling dynamics goes on exactly as discussed in Secs. III and IV, as if there is no noise at all.

On the other hand, in prospective technologies at borders with polymer physics, such as the emerging molecular nanotechnology, the aforementioned noise effects might be interesting due to the use of molecular rods with relatively small bending rigidity κ (compared to common mechanical engineering standards). There, for example, for small enough strains ε, one can easily encounter the floppy chains with $N>\lambda_{\max}=\varepsilon L_p$. Because of the potential interest for fine technologies, we also examined such chains by simulating their noisy Langevin buckling dynamics [Eq. (3.1)]. Thus in Fig. 6 we depict the behavior of the average internal strain e versus time. We see that $\langle e\rangle$ actually changes its sign from a negative value at short times $t<t_{\max}$ to a *positive* value at long times $t>t_{\max}$. At long times, $\langle e\rangle$ saturates to a positive value e_{eq}[$\langle e\rangle\approx e_{eq}$ for $t>t_{\max}$; see Fig. 6]. Apparently, by looking at *local* quantities, such as $\langle e\rangle$, the chain approaches

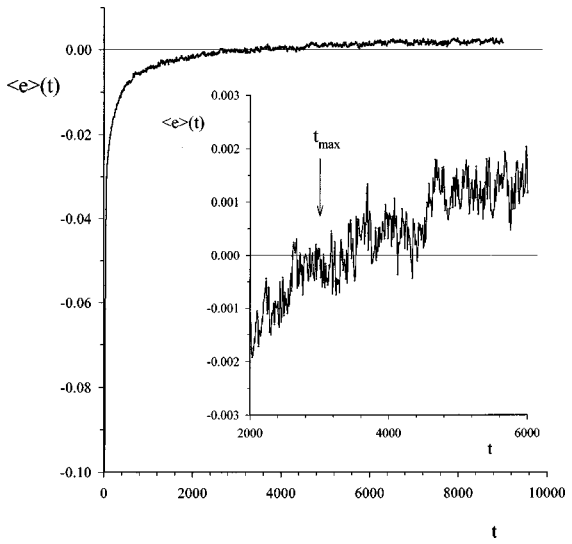

FIG. 6. Evolution of the internal strain $\langle e\rangle$ vs time t for the floppy chain with a relatively small time scale $t_{\max}$ ($\approx$3000 here) at which the internal strain changes from a negative to a positive value due to thermal noise.

its *thermal equilibrium* for $t>t_{\max}$. On the other hand, by looking at essentially nonlocal quantities such as $w(t)$ depicted in Fig. 7(a), we see that the chain roughness continues to grow for $t>t_{\max}$. As discussed in the Appendix, for $t \gg t_{\max}$, the system can be described by a noisy version of Eq. (4.7) with e replaced with a *positive* internal strain $e_{\rm eq}$. That is,

$$\Gamma \frac{\partial \vec{R}_\perp}{\partial t} = \sigma \cdot \frac{\partial^2 \vec{R}_T}{\partial n^2} - \kappa \frac{\partial^4 \vec{R}_T}{\partial n^4} + \vec{\eta}(n,t), \tag{6.6}$$

where σ is an entropically generated chain tension, given by

$$\sigma = B e_{\rm eq} = \frac{\kappa}{\lambda_\sigma^2} \tag{6.7}$$

Here $\lambda_\sigma \approx \lambda_{\max}$ at low temperatures, as discussed in the Appendix. By using Eq. (6.6), it can be easily shown that the chain roughness $w(t)$ continues to grow as $t^{1/4}$ even for $t>t_{\max}$, until it reaches its equilibrium value $w_{\rm eq} \sim (N)^{1/2}$ at another time scale $t_{\rm eq}=t_{\max}(N/\lambda_{\max})^2$, which is long if $N \gg \lambda_{\max}$. Simulation results in Fig. 7(a) document such behavior of $w(t)$, with $w(t) \sim t^{1/4}$ for $t_{\max} < t \ll t_{\rm eq}$. For $t>t_{\max}$, the internal strain $\langle e\rangle$ is *positive*, and the growth of $w(t)$ for $t>t_{\max}$ is driven by *thermal fluctuations* (thermal roughening). This is in contrast to the growth of $w(t)$ for $t<t_{\max}$ which is driven by a negative internal strain, as discussed in Secs. III and IV. For $t>t_{\max}$, the growth of $\lambda(t)$ slows down, as documented in Fig. 7(b). Figure 8(a) gives the slope-slope correlation function $K_{\rm ss}(r,t)$ in this noise dominated regime [as before, in Sec. III, its first zero was used to extract $\lambda(t)$]. By comparing this correlation function with strain dominated correlations in Fig. 2(a), it is obvious that, in the noise dominated regime, the chain configurations must be more disordered than in the strain dominated regime when the chain was periodic like [Fig. 1(b)]. In fact, a direct look at a chain configuration in the noise dominated regime confirms this; see Fig. 8(b). The chain profile has the random

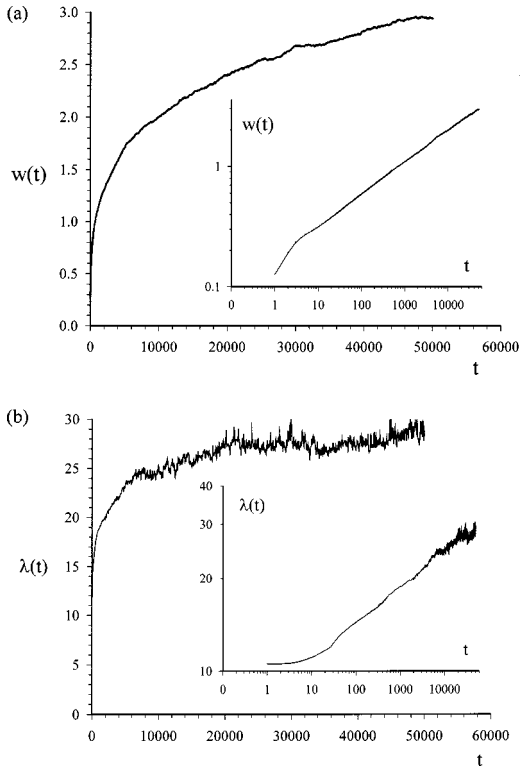

FIG. 7. (a) The time evolution of the chain transverse width $w(t)$ for the floppy chain in Fig. 8(b), $w(t) \sim t^{1/4}$ for both $t<t_{\max}$ ($\approx$3000 here) and $t>t_{\max}$. (b) The time evolution of the chain wavelength $\lambda(t)$ for the same floppy chain as in Fig. 8(b), $\lambda(t) \sim t^{1/4}$ for $t<t_{\max}$. For $t>t_{\max}$, the growth of $\lambda(t)$ slows down.

walk character of a directed polymer. This can be qualitatively explained by invoking Eq. (6.6), which can be solved exactly. For the displacement-displacement difference correlation function, it yields

$$K(r,t) \sim \sqrt{r} \tag{6.8}$$

for $r \ll \xi(t) = (\sigma t/\Gamma)^{1/2} = \lambda_{\max}(t/t_{\max})^{1/2} \sim t^{1/2}$, and

$$K(r,t) \approx \sqrt{2} w(t) \sim \sqrt{\xi(t)} \sim t^{1/4} \tag{6.9}$$

for $r \gg \xi(t)$. Thus, in contrast to the strain dominated regime, where we had, for $r \ll \lambda$, $K(r,t) \sim r^\alpha$ with $\alpha=1$ [see Fig. 3 and Eqs. (3.13) and (3.14)], in the noise dominated regime one finds, for $\lambda \ll r \ll \xi$, the random walk behavior $K(r,t) \sim r^\alpha$ with $\alpha \approx 0.5$. Figure 9, from our simulations of floppy chains, documents this behavior.

As noted before, for common mechanical engineering, the length scale $\lambda_{\max}$ is always much larger than sizes N of realistic systems. There, the noisy behavior described above is not accessible. Rather, one has just the coarsening driven by negative internal strains inducing a growth of λ according to $\lambda \sim t^{1/4}$. It lasts until a long time scale ($\sim N^{1/n_c}=N^4$) when the wavelength becomes comparable to the rod's size N, and one recovers the usual picture of a buckled rod. Interestingly, this noiseless coarsening dynamics of the buckling instability is still apparently stochastic. Chain nonlinearities and the presence of many degrees of motion (rather than noise) conspire to produce essentially *chaotic* chain dynamics. We recall that the only randomness that was used in the simula-

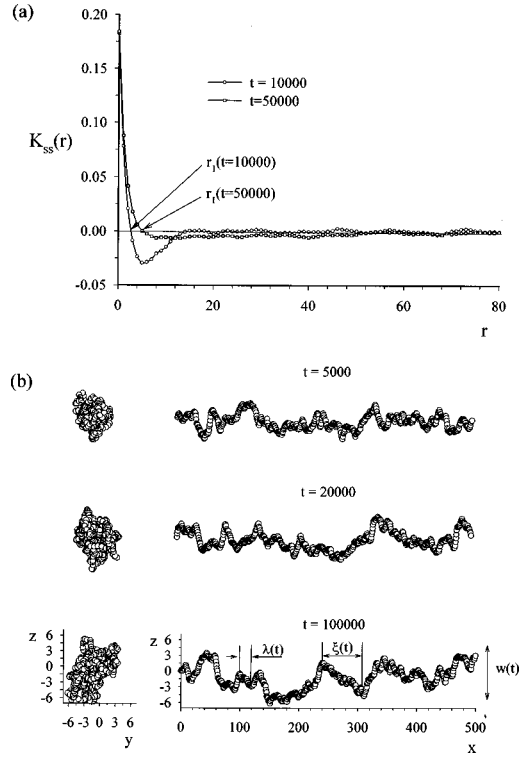

FIG. 8. (a) The slope-slope correlation functions $K_{ss}(r,t)$ at $t=10\,000$ and 50 000 for the floppy chain. (b) Time evolution of the floppy chain. We depict 550 out of 10 000 molecules comprising the chain. To depict undulations $\vec{R}_T(n,t)$ clearly, we used different scales for the transverse $\vec{R}_T=(R_y,R_z)$ and longitudinal $R_L=R_x$ molecular coordinates.

tions of Sec. III was small *initial* random transverse displacements around a straight unstable molecular configuration (to enable chain start moving). Subsequently, buckling instability, due to negative internal strains, amplifies the displacements and produces a chaotic coarsening described in Secs. III and IV.

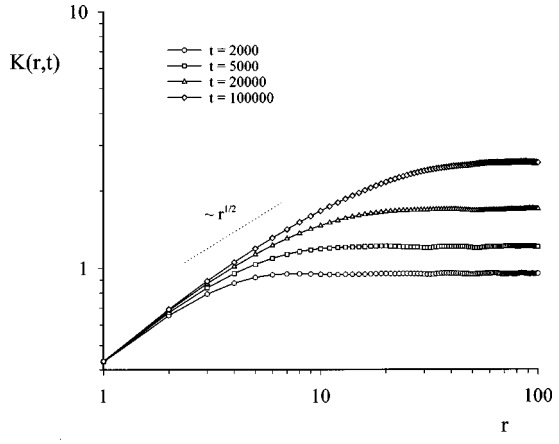

FIG. 9. The displacement-displacement difference correlation functions $K(r,t)$ for the floppy chains at various times. As discussed in the text, $K(r,t)\sim r^{\alpha}$ with $\alpha=\frac{1}{2}$, for $r\ll\xi(t)\sim t^{1/2}$, whereas $K(r,t)\cong\sqrt{2}w(t)\sim[\xi(t)]^{\alpha}\sim t^{1/4}$ for $r\gg\xi(t)$, as documented in Fig. 7(a). Numerically, $\alpha\approx 0.5$.

VII. SUMMARY AND DISCUSSION OF RELATED WORK

To summarize, here we have elucidated, in depth, the nature of the dynamics associated with the classical Euler instability. It is a coarsening process characterized by a growing structural length scale $\lambda(t)\sim t^{n_c}$. At long times ($\sim L^{1/n_c}$) this length scale becomes comparable to the rod length L, and one recovers the usual picture of a buckled rod. We reveal that the dynamics of Euler instability has the nature of a phase ordering process [8,9]: It is a stochastic coarsening process statistically self-similar in time. As in phase ordering phenomena, stochastic coarsening dynamics here occurs even in the absence of any noise, as a result of chain nonlinearities and the presence of many degrees of freedom. Associated with this coarsening process is the *growing transverse width* of the rod $w(t)\sim t^{\beta}$, with $\beta=n_c$. Such a growth of $w(t)$, with $\beta=n_c$, is similar to the interfacial coarsening process recently found to occur in molecular beam epitaxy (so-called pyramidal or mound growth [10–12]). There, as well as in the present elastic problem, the evolving manifold (surface or line) develops a nonzero slope with respect to the initial straight configuration. The chain slope plays the role of the order parameter in this phase ordering phenomenon.

It is interesting to note that the growth of the chain wavelength in Eq. (4.15) is similar to the well known $\frac{1}{4}$ power law of the subdiffusive spreading of a transverse disturbance along a flexible chain in the *absence* of external tension, as obtained within linearized elastohydrodynamics [18]; see Eq. (4.8), with $\varepsilon=0$. The spreading process is associated with a *decay* of transverse chain displacements that justifies the use of the linearized theory at long times. On the other hand, buckling is associated with the *growth* of chain transverse displacements that leads to a *breakdown* of linearized theory (see Sec. IV). Thus the similarity of chain buckling dynamics and the linearized elastohydrodynamics is *accidental*. This is best illustrated by our recent work on the buckling dynamics of *tethered membranes* [7]: As in polymers, the Rouse dynamics of tethered membranes exhibits the standard $\frac{1}{4}$ power law for the spreading of a disturbance. Nonetheless, in the buckling regime, the coarsening exponent n_c for tethered membranes is not $\frac{1}{4}$. Rather, $\lambda(t)\sim t^{n_c}$ with $n_c=\frac{3}{11}$, for Rouse buckling dynamics of tethered membranes [7]. This difference arises due to the development of ridge networks across buckling membranes [7], as noted above in Sec. V.

We note that a $\frac{1}{4}$ power law was found in Ref. [15], in the straightening process of flexible polymers under tension applied to one end of the polymer. It has been found that the size of the straightened (tense) region grows, under some conditions, by a $\frac{1}{4}$ power law, with a prefactor different from that in Eq. (4.15). In fact, the nature of this straightening power law is different from that of the coarsening law that applies to buckling dynamics. For example, in contrast to Eq. (4.15), the overall form of the straightening power law depends on the initial chain configuration, e.g., on the initial chain temperature [15]. Furthermore, the straightening dynamics exhibiting the $\frac{1}{4}$ power law occurs even for zero bending rigidity [15], in contrast to buckling dynamics, in which chain bending rigidity plays the central role. Even with bending rigidity included into the dynamics, the straightening remains substantially different from buckling. The buckling has the character of a phase ordering process,

with the chain slope as the order parameter. Straightening on the other side does not have such a character.

ACKNOWLEDGMENTS

We thank Andrew Karwowski and Arnoud Saint-Jalmes for discussions. This research was supported by Mylan Laboratories, Inc. and by NSF/WV EPSCoR.

APPENDIX

Here we discuss Eq. (6.6) and related issues of Sec. VI. For this purpose, here we discuss the equilibrium statistical mechanics of the flexible chain of molecules with the elastic energy as in Eqs. (4.4)–(4.6), that is,

$$U(\vec{R}_T,u')=\int_0^N dn\left\{\frac{B}{2}\left[-\varepsilon+\frac{\partial u'}{\partial n}+\frac{1}{2}\left(\frac{\partial \vec{R}_T}{\partial n}\right)^2\right]^2+\frac{\kappa}{2}\left(\frac{\partial^2\vec{R}_T}{\partial n^2}\right)^2\right\}. \tag{A1}$$

Here, as in Sec. IV, $u'(n)$ are phonons, whereas $\vec{R}_T(n)$ is a $d-1=2$ component field of chain transverse displacements [for generality, we consider a chain fluctuating in a d-dimensional space]. Next consider the partition function associated with Eq. (A1),

$$Z=\int DR_T\int Du'\,e^{-U(R_T,u')/k_BT}. \tag{A2}$$

As Eq. (A1) is harmonic in the phonons u', they can be integrated out of the partition function (A2) exactly, yielding $Z\sim\int DR_T e^{-U_{\rm eff}(\vec{R}_T)/k_BT}$, where $U_{\rm eff}(R_T)$ is obtained by minimizing Eq. (A1) over the phonons $u'(n)$ for fixed $\vec{R}_T(n)$. The condition $\delta U/\delta u'=0$ yields the equation

$$0=\frac{\partial}{\partial n}\left[-\varepsilon+\frac{\partial u'}{\partial n}+\frac{1}{2}\left(\frac{\partial\vec{R}_T}{\partial n}\right)^2\right]. \tag{A3}$$

From Eq. (A3),

$$-\varepsilon+\frac{\partial u'}{\partial n}+\frac{1}{2}\left(\frac{\partial\vec{R}_T}{\partial n}\right)^2=C, \tag{A4}$$

where C is an integration constant to be fixed from the boundary conditions. In this case, they are: $u'(n=0)=0$ and $u'(n=N)=0$ (fixed chain ends), implying

$$\int_0^N dn\,\frac{\partial u'}{\partial n}=0, \tag{A5}$$

as already discussed in Sec. IV, see Eq. (4.1). From Eqs. (A4) and (A5),

$$C=\frac{1}{N}\int_0^N dn\left[-\varepsilon+\frac{1}{2}\left(\frac{\partial\vec{R}_T}{\partial n}\right)^2\right]. \tag{A6}$$

Note that, from Eqs. (A3) and (A4), the phonon configuration minimizing the elastic energy yields uniform (constant) strain [Eq. (4.3)] along the chain. By inserting this phonon configuration into Eq. (A1), we obtain

$$U_{\rm eff}(R_T)=\frac{B}{2}\cdot\frac{1}{N}\left\{\int_0^N dn\left[-\varepsilon+\frac{1}{2}\left(\frac{\partial\vec{R}_T}{\partial n}\right)^2\right]\right\}^2+\frac{\kappa}{2}\int_0^N dn\left(\frac{\partial^2R_T}{\partial n^2}\right)^2, \tag{A7}$$

as the effective free energy functional for chain undulations $\vec{R}_T(n)$. The first term in Eq. (A7) is an *infinite* range interaction between chain undulations which is mediated by phonons. Its presence makes Eq. (A7) similar to the Kac model of ferromagnets with infinite range exchange interactions [19]. Here, as in the case of the standard Kac model, the presence of the infinite range interactions makes the equilibrium statistical mechanics exactly solvable in the thermodynamic limit $N\to\infty$. By treating Eq. (A7) in a fashion similar to that used for the Kac model, we find that the equilibrium correlations of chain undulations $[\vec{R}_T(n)]$ can be obtained from an effective Hamiltonian of the form

$$H_0(R_T)=\frac{\sigma}{2}\int_0^N dn\left(\frac{\partial\vec{R}_T}{\partial n}\right)^2+\frac{\kappa}{2}\int_0^N dn\left(\frac{\partial^2\vec{R}_T}{\partial n^2}\right)^2. \tag{A8}$$

Here σ is the *equilibrium* chain tension, which satisfies the equation

$$\sigma=B\langle e\rangle_0=B\left\langle-\varepsilon+\frac{1}{2}\left(\frac{\partial\vec{R}_T}{\partial n}\right)^2\right\rangle_0, \tag{A9}$$

where the average is with respect to $H_0(R_T)$ in Eq. (A8). This yields a self consistent equation for the chain tension of the form

$$\sigma=B\left[-\varepsilon+\frac{d-1}{2}\int\frac{dq}{2\pi}\frac{k_BT}{\sigma+\kappa q^2}\right]. \tag{A10}$$

Once Eq. (A10) is solved for σ, the equilibrium value of the internal strain, $e_{\rm eq}=\langle e\rangle$, is from Eq. (A9),

$$e_{\rm eq}=\langle e\rangle_0=\frac{\sigma}{B}. \tag{A11}$$

By performing the momentum integral in Eq. (A10), we obtain the equation

$$\sigma=B\left[-\varepsilon+\frac{d-1}{4}\frac{k_BT}{\sqrt{\sigma\kappa}}\right], \tag{A12}$$

to be solved for σ. By solving Eq. (A12), we find the chain tension in the form

$$\sigma=Be_{\rm eq}=\frac{\kappa}{\lambda_\sigma^2}. \tag{A13}$$

Here λ_σ is a tension related length scale given by

$$\lambda_\sigma\cong\begin{cases}\lambda_{\max} & \text{for } T\ll T_{\rm buck},\\ \tilde{\lambda} & \text{for } T\gg T_{\rm buck}.\end{cases} \tag{A14}$$

In Eq. (A14),

$$\lambda_{\max}=\varepsilon L_p, \tag{A15}$$

where L_p is the free chain persistence length,

$$L_p=\frac{4}{d-1}\frac{\kappa}{k_BT}, \tag{A16}$$

as in Sec. VI. $\tilde{\lambda}$ in Eq. (A14) is given by

$$\tilde{\lambda}=\left(\frac{4}{d-1}\frac{\kappa^2}{Bk_BT}\right)^{1/3}. \tag{A17}$$

$T_{\rm buck}$ in Eq. (A14) is a characteristic ''buckling'' temperature scale, given by

$$k_BT_{\rm buck}=\sqrt{\kappa B\varepsilon^3}. \tag{A18}$$

The significance of the temperature scale $T_{\rm buck}$ for the noisy buckling dynamics (Sec. VI) can be seen by forming the ratio $\lambda_{\max}/\lambda_0$, where λ_0 is the initial ($t=0$) value of the chain wavelength, $\lambda_0=\text{const}\sqrt{\kappa/B\varepsilon}$; see Eq. (4.10). From Eqs. (A15) and (A16), one has

$$\frac{\lambda_{\max}}{\lambda_0}=\text{const}\frac{T_{\rm buck}}{T}. \tag{A19}$$

Thus, for $T\ll T_{\rm buck}$, one has $\lambda_{\max}\gg\lambda_0$. In terms of the noisy chain dynamics of Sec. VI, for $T\ll T_{\rm buck}$ one has a broad range of time scales exhibiting the zero-temperature buckling dynamics

$$t_0<t<t_{\max}, \tag{A20}$$

with

$$t_{\max}=\left(\frac{\lambda_{\max}}{\lambda_0}\right)^4 t_0=\left(\frac{T_{\rm buck}}{T}\right)^4 t_0. \tag{A21}$$

As discussed in Sec. VI, for t in range (A20), the coarsening proceeds as in the absence of the thermal noise ($T=0$), with $\lambda(t)\sim t^{1/4}$. For $t<t_{\max}$, the coarsening is driven by the negative internal strain $\langle e\rangle_t$. The internal strain $\langle e\rangle_t$ changes its sign at $t=t_{\max}$, and, at long times, approaches its positive equilibrium value $e_{\rm eq}$ given by Eq. (A13). Such an evolution of $\langle e\rangle_t$ is illustrated by our simulations; see Fig. 6. For $t>t_{\max}$, the chain approaches its thermodynamic equilibrium, and its dynamics can be qualitatively described by the linearized noisy Langevin dynamics in Eq. (6.6), which brings the system into the equilibrium state governed by the effective Hamiltonian in Eq. (A8). For $t>t_{\max}$, the internal strain $\langle e\rangle_t$ is positive, and the chain has a roughening dynamics driven by thermal noise. This late time dynamics ($t>t_{\max}$) is essentially that of directed polymers under an entropically generated positive tension σ, as in Eq. (6.6). Simulations of the full nonlinear noisy Langevin dynamics [Eq. (3.1)] corroborate this picture (see Sec. VI).

Finally, we note that the range of time scales in Eq. (A20) is, by Eq. (A21), broad only for $T\ll T_{\rm buck}$. Only then does one have a broad range of time scales in Eq. (A20), in which the buckling dynamics is driven by negative internal strains and goes as at $T=0$, with $\lambda(t)\sim t^{1/4}$, as discussed in Secs. III and IV. From Eq. (A21), this zero-T-like regime should disappear for $T>T_{\rm buck}$. Above $T_{\rm buck}$, the time scale $t_{\max}$ is short ($t_{\max}\approx t_0$), and the subsequent chain dynamics has only a noisy dominated regime with a positive internal strain and thermally induced roughening.

[1] L. D. Landau and E. M. Lifshitz, *Theory of Elasticity* (Pergamon, New York, 1986); A. E. Love, *A Treatise on the Mathematical Theory of Elasticity* (Dover, New York, 1944).

[2] J. P. Den Hartog, *Strength of Materials* (Dover, New York, 1977).

[3] See MRS Bull. **21** (4), 18 (1996), special issue on heteroepitaxy and strain, edited by Leo J. Schowalter.

[4] L. Bordieu, J. Daillant, D. Chatenay, A. Braslau, and D. Colson, Phys. Rev. Lett. **72**, 1502 (1994); A. Saint-Jalmes and F. Gallet, Eur. Phys. J. B **2**, 498 (1998).

[5] A. M. Huntz, Mater. Sci. Eng., A **201**, 211 (1995).

[6] L. Golubovic, D. Moldovan, and A. Peredera, Phys. Rev. Lett. **81**, 3387 (1998).

[7] D. Moldovan and L. Golubovic, Phys. Rev. Lett. **82**, 2884 (1999), and Phys. Rev. E **60**, 4377 (1999) address the buckling dynamics of tethered membranes.

[8] H. Furukawa, Adv. Phys. **34**, 703 (1985); K. Binder, Rep. Prog. Phys. **50**, 783 (1987).

[9] A. J. Bray, Adv. Phys. **43**, 357 (1994).

[10] H.-J. Ernst, F. Fabre, R. Folkerts, and J. Lapujoulade, Phys. Rev. Lett. **72**, 112 (1994); M. D. Johnson, C. Orme, A. W. Hunt, D. Graff, J. Sudijono, L. M. Sander, and B. G. Orr, *ibid.* **72**, 116 (1994); J. Amar and F. Family, Phys. Rev. B **54**, 14 742 (1996); P. Smilauer and D. D. Vvedensky, *ibid.* **52**, 14 363 (1995).

[11] L. Golubovic and R. P. U. Karunasiri, Phys. Rev. Lett. **66**, 3156 (1991).

[12] L. Golubovic, Phys. Rev. Lett. **78**, 90 (1997).

[13] S. Edwards, Proc. Phys. Soc. London **88**, 265 (1966); L. Golubovic and W. Xie, Phys. Rev. E **51**, 2856 (1995).

[14] For a review, see *Statistical Mechanics of Membranes and Surfaces*, edited by D. R. Nelson, T. Piran, and S. Weinberg (World Scientific, Singapore, 1989).

[15] U. Seifert, W. Wintz, and P. Nelson, Phys. Rev. Lett. **77**, 5389 (1996).

[16] C. H. Wiggins and R. E. Goldstein, Phys. Rev. Lett. **80**, 3879 (1998); C. H. Wiggins, D. Riveline, A. Ott, and R. E. Goldstein, Biophys. J. **74**, 1043 (1998).

[17] R. Goldstein, T. R. Powers, and C. H. Wiggins, Phys. Rev. Lett. **80**, 5232 (1989).

[18] See, e.g., Ref. [16], and references therein.

[19] H. E. Stanley, *Introduction to Phase Transition and Critical Phenomena* (Oxford University Press, New York, 1987), Chap. 6.